Symmetrically Disubstituted Bithiophene Derivatives of 1,3,4-Oxadiazole, 1,3,4-Thiadiazole and 1,2,4-Triazole – Spectroscopic, Electrochemical and Spectroelectrochemical Properties

Aleksandra Kurowska [a,#], Anastasia S. Kostyuchenko [b,c,#], Pawel Zassowski [a], Lukasz Skorka [d], Viacheslav L. Yurpalov [b], Alexander S. Fisyuk [b,c], Adam Pron [d], Wojciech Domagala [a,]*

[a] Department of Physical Chemistry and Technology of Polymers, Silesian University of Technology, Marcina Strzody 9, 44-100 Gliwice, Poland

[b] Department of Organic Chemistry, Omsk F. M. Dostoevsky State University, Mira ave. 55A, Omsk 644077, Russian Federation

[c] Laboratory of New Organic Materials, Omsk State Technical University, Mira ave. 11, Omsk 644050, Russian Federation

[d] Faculty of Chemistry, Warsaw University of Technology, Noakowskiego 3, 00-664 Warszawa, Poland

\# First two authors contributed equally to this work

* corresponding autor, e-mail: wojciech.domagala@polsl.pl

tel: (+48) 32-2371305

fax: (+48) 32-2371925

Abstract

Electrochemical and spectroelectrochemical properties of a series of new penta-ring donor – acceptor compounds, comprising 1,3,4-oxadiazole, 1,3,4-thiadiazole and 1,2,4-triazole central ring, symmetrically connected to substituted bithiophenes, were investigated. Aromaticity and electrophilic - nucleophilic traits of the aza-heterocyclic units, fostering inductive and resonance effects that translate to conjugation enhancement and electron (de)localization, were found a major factor determining the key electron properties of ionization potential (IP) and electron affinity (EA) of these molecules. Replacing the alkyl thiophene substituent for an alkoxy one, afforded certain control over the two parameters as well. All studied compounds were found to undergo electrochemical polymerization giving *p* and *n*-dopable products, featuring good electrochemical reversibility of their oxidative doping process, as demonstrated by cyclic voltammetry and UV-Vis-NIR, EPR spectroelectrochemistry. While electropolymerisation of entities differing in the heterodiazole unit was found to conserve the EA value, the IP parameter of polymerisation products was found to decrease by 0.6 to 0.7 eV affording an asymmetric narrowing of the frontier energy levels gap. Aided by quantum chemical computations, the effects of structure tailoring of the investigated systems are rationalized, pointing to conscious ways of shaping the electronic properties of thiophene class polymers using synthetically convenient heterodiazole π-conjugated units.

1. Introduction

In recent years low and high molecular weight organic semiconductors received great attention because of their potential applications in such electronic and electrochemical devices as photovoltaic cells (PCs), photodiodes (PDs), light emitting diodes (LED's), field effect transistors (FETs), and various types of sensors and electrochromic devices.[1–11]

Appropriate functionalization of these compounds make them solution processable and allows for precise tuning of their electronic, spectroscopic, electrochemical and mechanical properties. For example, molecules exhibiting high electron affinity (|EA|>3.9 eV) due to their low lying LUMO level are good candidates for the fabrication of air operating n-channel FETs.[7] Organic semiconductors of appropriate ionization potential (5.5>IP>5.1 eV) are, in turn, the best suited for p-channel FETs.[7] Semiconductors for ambipolar transistors and for photovoltaic cells should fulfill both above listed conditions.[11] Thus, broad absorption spectrum and a low band gap are greatly desired for many of these applications.[1,12,13]

Functionalized oligothiophenes and polythiophenes constitute an interesting class of organic semiconductors, however for many applications their IP is not appropriate and their band gap too large. Band gap narrowing with simultaneous increase of IP is usually achieved by synthesizing donor/acceptor molecules of AD, DAD or ADA types or their polymeric analogues.[4,14,15] In these cases narrower band gap results from mesomeric effects, which are responsible for an increase of the double bond character between the donor and acceptor units.[1,16,17]
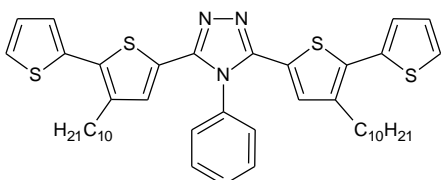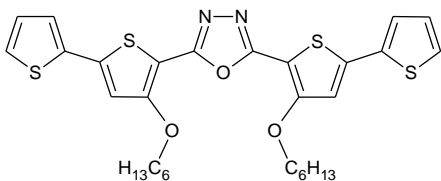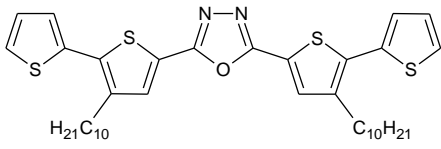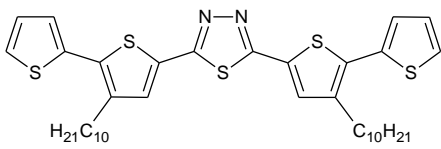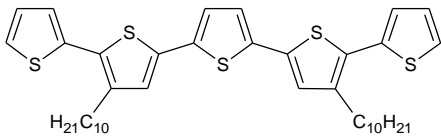
The above outlined strategy can also be applied to the synthesis of molecules showing IP significantly higher than that of oligothiophenes. In such compounds a central strongly electron accepting unit of tetrazine-[18–21], thiadiazole-[22,23] or oxadiazole- type bridges two bi- or

terthiophene segments.[24] In this report we describe new five-ring donor-acceptor-donor compounds of D_1-D_2-A-D_2-D_1), where D_1 and D_2 stand for nonsubstituted and substituted thiophene ring and A – for 1,3,4-oxadiazole or 1,3,4-thiadiazole or 1,2,4-triazole. In particular we discuss the effect of the nature of the central electron accepting unit and the solubilizing substituent on the redox, spectroscopic and spectroelectrochemical behavior of these compounds. Electrochemical determination of the redox properties of these new semiconductors is of crucial importance in view of the fact that some of them show strong electroluminescence and can be used as components of light emitting diodes with tunable colors .[25] Moreover, they readily undergo oxidative, electrochemical polymerization, yielding macromolecular compounds which show very interesting UV-Vis-NIR and EPR spectroelectrochemical response. The experimental findings reported here are theoretically supported by DFT calculations.

2. Experimental

Investigated compounds comprise different diazole central electron accepting unit symmetrically substituted with alkyl or alkoxy functionalized electron donating bithiophene group. Three different diazole units: 1,2,4-triazole, 1,3,4-oxadiazole and 1,3,4-thiadiazole, were chosen as core acceptor units. The structural formulae of all four donor-acceptor systems together with a quinquethiophene reference derivative considered theoretically herein, are presented in Table 1.

Table 1 - Chemical formulae of experimentally and theoretically investigated compounds.

Signature	Structure	Systematic name
1		3,5-*bis*(3-decyl-2, 2'-bithien-5-yl)-4-phenyl-4H-1,2,4-triazole
2		2,5-bis[4-(hexyloxy)-2,2'-bithien-5-yl]-1,3,4-oxadiazole
3		2,5-*bis*(3-decyl-2,2'-bithiophene-5-yl)-1,3,4-oxadiazole
4		2,5-*bis*(3-decyl-2,2'-bithiophene-5-yl)-1,3,4-thiadiazole
5		3',4$^{3'}$-bisdecyl-2,2':5',2'':5'',2$^{3'}$:5$^{3'}$,2$^{4'}$-quinquethiophene

Compounds (**1**) through (**4**) studied experimentally have been synthesized in our group. The synthesis of (**4**) was reported previously.[26] The synthetic pathways undertaken to obtain all four investigated compounds, three of which are new, are discussed in [27].

2.1 Electrochemical, spectroscopic and spectroelectrochemical investigations

All electrochemical measurements were performed in 0.1M Bu_4NPF_6 (Sigma-Aldrich) in dichloromethane (Sigma-Aldrich, for HPLC), using an Autolab PGSTAT20 potentiostat (EcoChemie, Netherlands). All solutions were purged with argon prior to the electrochemical experiments. The electrochemical cell consisted of a platinum working electrode, a platinum wire counter electrode and an Ag wire pseudo-reference electrode. The potential of the pseudo-reference electrode was calibrated in the same electrolytic solution *versus* ferrocene redox couple after each experiment. The values of the potentials listed in this work are given with respect to the ferrocene redox couple if not stated otherwise. Cyclic voltammetry – driven electropolymerisations were carried in 1mM solutions of a given monomer, using the scan rate of 100 mV/s. For further investigations (redox behavior, spectroelectrochemistry), the electrode with the obtained deposit was repeatedly washed with a pure solvent and then transferred into a cell containing a monomer-free electrolyte.

Photoluminescence spectra of the monomers were obtained on a Hitachi F-2500 fluorescence spectrometer. The optical energy gaps, corresponding to the energy difference between HOMO and LUMO levels of monomers dissolved in dichloromethane, were estimated from the onset of the π-π* absorption band. The fluorescence excitation spectra were recorded for the emission maximum and the fluorescence emission spectra were recorded for the excitation

maximum. The quantum yield of the examined compounds was estimated by comparison with a quantum yield standard using comparative method.[28] In this case, the quantum yield is calculated according to the following equation:

$$\Phi = \Phi_R \cdot \left(\frac{m}{m_R}\right) \cdot \left(\frac{n^2}{n_R^2}\right)$$

where: Φ is the quantum yield, m is the slope of origin approaching linear segment of the plot of integrated fluorescence intensity vs. absorbance of a fluorophore solution plot, n is the refractive index of solvent and subscript R refers to data for the solution of reference fluorophore of known quantum yield – in this case: 9,10-diphenylanthracene in ethanol (Φ_R=0.950 for excitation at 330-380 nm) and in cyclohexane (Φ_R=0.955 for excitation at 366 nm).[29]

Spectroelectrochemical investigations were carried out using Ocean Optics QE65000 and NIRQuest512 diode array spectrometers. In these experiments the electropolymerization products were deposited on an ITO transparent electrode in the same conditions as in the case of the electropolymerization on platinum (*vide supra*). The UV-Vis-NIR spectra were obtained in a 2 mm quartz cuvette and recorded in the increasing electrode potential mode.

Electron paramagnetic resonance (EPR) measurements were performed using a JEOL JES-FA200 spectrometer coupled with an Autolab PGSTAT 100N potentiostat. EPR spectra were acquired at a microwave power of 1mW. For these investigations thin polymer layers were deposited onto a platinum wire using the same conditions as in the two previously mentioned cases (cyclic voltammetry and UV-Vis spectroelectrochemistry). All measurements were performed in a custom-made electrochemical glass cell narrowed at the bottom to provide proper, thin electrolyte layer measurement conditions. The EPR spectra were recorded in increasing electrode potential mode. Relative number of paramagnetic centers was determined by double integration of the obtained spectra. g-Factor of spins generated during the oxidative doping of the

investigated polymers was determined by comparison with JEOL internal standard (Mn(II) salt), knowing that its 3rd hyperfine line has a g-factor of 2.03323.

2.2 DFT Calculations

DFT calculations were carried out using Gaussian09 Revision D.01 [30] package and employing hybrid B3LYP [31–33] exchange correlation potential combined with 6-31G(d,p) basis set. Ground-state geometries were fully optimized until a stable local minimum was found, which was confirmed by normal-mode analysis (no imaginary frequencies were present). Symmetry constrains were used wherever possible imposing C_2 point group. The ground-state geometries were then re-optimized in solution using polarizable continuum model (PCM) [34] at the same level of theory, with dichloromethane as a solvent. The oscillator strengths and energies of the vertical singlet excitations were calculated employing the time-dependant version (TD) of DFT [35–41] and again at the same level of theory (B3LYP/6-31G(d,p)). The TD-DFT results were retrieved from output files using GaussSum 2.2.[42] Molecular orbital plots were generated with the aid of Gabedit 2.4.6.[43] Singlet excited to ground state vertical electronic transitions were calculated taking into account the Franck-Condon rule and state-specific solvation of the excited state.[44,45] Analysis of electropolymers was carried out with the aid of periodic boundary conditions (PBC/B3LYP/6-31G(d,p)).[46,47]

3. Results and discussion

3.1 Spectroscopy of monomers: theory *versus* experiment

Five-ring compounds consisting of an electron-accepting heterocyclic ring symmetrically end-capped with bithiophene containing an alkyl (or alkoxy) solubilising group, in their UV-Vis

spectra give rise to one unresolved band, ascribed to the π- π* transition in the conjugated system. Its position depends on the chemical nature of the central heterocyclic ring and the solubilising substituent (alkyl *vs* alkoxy). To a lesser extent, it also depends on the position of the substituent[23] (see Figure 1a and Table 2). The transition in the thiadiazole derivative (**4**) is the least energetic of all four studied compounds, implying the lowest optical band gap (2.64 ± 0.01 eV). The first conclusion would be to assign this result to the stronger electron accepting properties and higher aromaticity of thiadiazole compared to the other heterocyles (oxadiazole and triazole.[48,49]). Optical transitions only provide information about the breadth of frontier orbitals separation. When the individual redox transformations of this compound are probed electrochemically the situation turns out a little more complex (*vide infra*). What is certain is that the increasing red-shift of the absorption band observed for (**3**), (**2**) and (**4**), as compared to (**1**), can be associated with increasing aromaticity[4,48,50] of the 3,4-diazole heteroatomic ring together with promoted delocalization of π-electron density between the bithiophene units.

One should also note that replacement of an alkyl substituent by an alkoxy one slightly lowers the optical band gap by 0.15 eV in (**2**) as compared to (**3**), due to the more evident electron-donating property of the alkoxy chain which causes elevation of the molecule HOMO level and, by consequence, narrowing of the band gap.

The aforementioned phenomena were examined by means of TD-DFT calculations. They were performed on geometries optimized in dichloromethane solution imposing C_2 symmetry. It was found that the exclusive contribution to the most intense band in the spectrum is associated with only one transition that is the HOMO→LUMO excitation evidenced by huge value of its oscillator strength. What may be straightforwardly extracted from the presented data is that the localization of the transition is strongly influenced by both the nature of the central ring and the substituent in the side thiophene rings. In particular, in the alkyl derivative of the oxadiazole

compound (**3**)**,** the HOMO to LUMO transition gives rise to a band at 412 ± 1 nm whereas the analogous transition in the alkoxy derivative (**2**) is bathochromically shifted to 461 ± 1 nm. Similar effect is spotted when the central oxadiazole ring is replaced by the thiadiazole moiety (a bathochromic shift to 451 nm in (**3**)). On the other hand, the incorporation of the triazole unit in the central part of the molecule slightly blue-shifts the absorption band to 400 ± 1 nm. That phenomenon implies that there is a significant torsion twist between the triazole and side thiophene rings , brought about by steric hindrance of the phenyl substitutent.[51] It leads to a reduction of the S_0/S_1 (π-π*) transition (λ_{max})by about 41 nm (0.35 eV) comparing two extreme cases (**1**) and (**4**) (Table 2).

The theoretical data do not strictly reproduce the experimental values, but the same trend in the absorption shift is observable. TD-DFT calculations give a good qualitative idea of the substituent effect on the electronic spectrum (see Table 3).
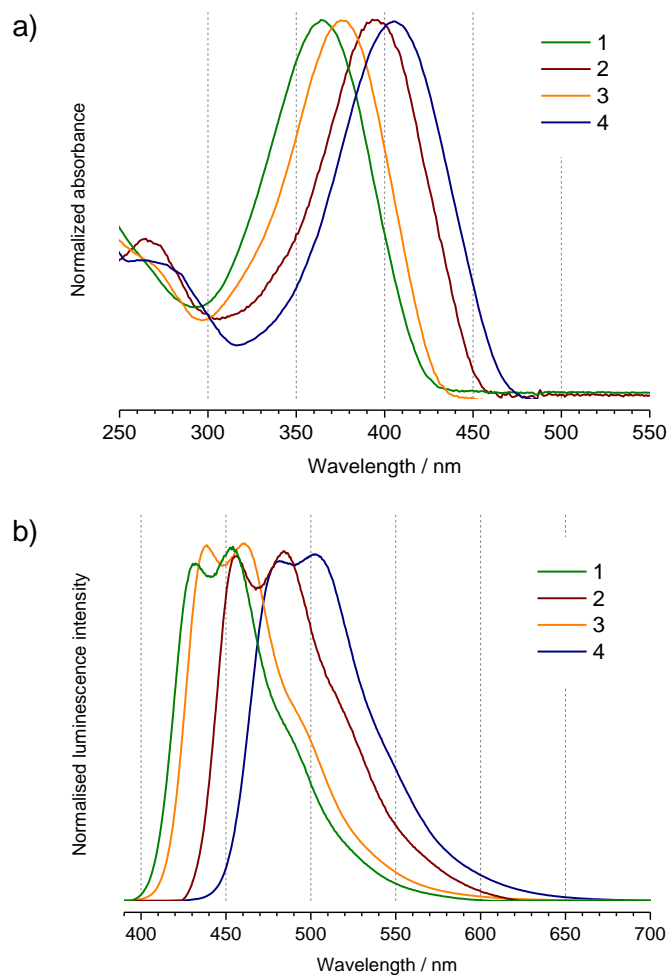
Figure 1 -a) Absorption and b) fluorescence spectra of dilute solutions of investigated compounds (1-4) in dichloromethane. Spectra of each type have been normalized arbitrarily to a common maximum.

All investigated di- and triazole derivatives are efficiently photoluminescent , reaching 0.59 quantum yield for (**1**). This value is strongly related to the kind of acceptor unit in monomer backbone. With increasing strength of acceptor moiety the quantum yield decreases. The significant increase of fluorescence quantum yield from 1,3,4-thiadiazole (0.21 ± 0.04) moiety to 1,3,4-oxadiazole (0.42 ± 0.04) can be explained by the heavy atom effect.[48,52] The replacement of sulfur/oxygen by the third nitrogen atom in the acceptor unit of (**1**) also increases the quantum yield ($\Delta\Phi_{1,3}=0.17$) whereas for the couple (**1**)/(**4**) ($\Delta\Phi_{1,4}=0.38$) the difference is more noticeable.

A comparison between the examined compounds reveals that the replacement by the more electronegative atom in heterocyclic ring leads to the blue-shift of emission maxima by about $\lambda^{em}_4 - \lambda^{em}_1 = 47$ nm, comparing the two extreme cases (Table 2, Figure 1b).

Contrary to the π-π^* absorption bands of investigated compounds, their emission bands feature vibronic structure with two discernable maxima and a shoulder (Figure 1b). This can be considered as an indication of higher planarity and stiffness of the excited state structures, which is also clearly evidenced by TD-DFT calculations The values of the Stokes shift between Δv=59-70 nm points to considerable geometric reorganization of the excited state compared to the ground state (Table 2).[48] Analyzing the data trends, the Stokes shift appears to be unrelated to the acceptor strength of the diazole moiety. as well as to the kind of pendant group substituted to the thienyl unit when comparing (**2**) with (**3**) (Table 2).[51] As aforementioned, clear vibronic structure in the emission bands is a typical manifestation of electron-lattice coupling. Observable transition from the ground state to the relaxed excited state is proportional to the conjugation length.[24] It should be noted that in case of (**4**) the band corresponding to that transition is significantly red-shifted as compared to the spectra of other molecules. This implies that insertion of the thiadiazole moiety into the molecule backbone significantly improves the conjugation length.

The emission spectra and their deconvolutions are given in Figure SI.1. The emission profile could be fitted with at least four bands for all examined compounds which correspond to fluorescence transitions ($S_0^{v=0} \rightarrow S_1^{v=0}$, $S_0^{v=0} \rightarrow S_1^{v=2}$, $S_0^{v=0} \rightarrow S_1^{v=3}$). Analyzing the deconvoluted emission spectra[53], the energy difference between the particular vibrational bands falls in the range of 1100 cm^{-1} - 1300 cm^{-1}, which corresponds to C=C symmetric stretch vibrations in heteroaromatic compounds (Table SI.1 - Supporting Information). It is noticeable that with the increasing strength of the acceptor unit the in molecule backbone, the 0-0 emission peak is red shifted. That phenomenon indicates that the relaxation energy in the excited state of (**4**) is smaller

compared with the other compounds (**1**-3). The difference between the most significant transition is $\Delta T^{0\text{-}0}_{2,4} = 0.02$ eV, comparing two extreme cases. The smallest energy difference between 1st and 2nd transition is obtained for (**4**) (0.152 eV) whereas the biggest difference is for (**2**) (0.172 eV) and (**1**) (0.160 eV). This indicates that during the vibrational relaxation more energy is lost in the case of (**2**) comparing to the other molecules.

Table 2 - UV-Vis and photoluminescence data for the studied pentaring compounds.

	UV-Vis		Photoluminescence			
Compound	$\lambda_{max}{}^{a}$ [nm]	H-L[eV]	$\lambda_{ex}{}^{a}$ [nm]	$\lambda_{em}{}^{b}$ [nm]	Stokes shift [nm]	Quantum yield
1	365	2.94	363	429; 454; 481	64	0.59 ± 0.04
2	395	2.72	382	454; 484; 519	59	0.45 ± 0.08
3	376	2.87	365	436; 461; 491	60	0.42 ± 0.04
4	406	2.64	373	476; 505; 537	70	0.21 ± 0.04

^{a} experimental error: ± 1 nm.
^{b} maxima obtained from deconvolution of the spectra (see Supporting Information Table SI.1)

Table 3 - First vertical excitation wavelengths, energies and oscillator strengths computed on B3LYP/6-31G(d,p) level of theory.

Compound	Wavelength (nm)	Energy (eV)	Osc. strength	Symmetry	Major contribution
1	400.28	3.10	1.4122	Singlet-B	HOMO→LUMO (99%)
2	460.97	2.69	1.3397	Singlet-B	HOMO→LUMO (99%)
3	412.11	3.01	1.3834	Singlet-B	HOMO→LUMO (99%)
4	450.80	2.75	1.405	Singlet-B	HOMO→LUMO (99%)

In order to investigate the nature of the excited-to-ground state transitions TD-DFT was used. The calculations were carried out employing the Franck-Condon rule for emission and moreover the solvent effects were accounted for *via* state-specific solvation of the excited state. The geometries of all four molecules were re-optimized in the search for energy-minimum structure of S_1 state in solution. Since the geometries corresponded to the excited state, the first singlet ground-to-excited state transitions were in fact equal to the emission energies computed *via* solvent reaction field of the ground state (linear response). Then the state-specific solvation was applied to get a more correct description of the excited state. Finally, the emission energy was determined as the difference between the excited and ground states imposing the geometry and reaction field from the excited state. The aforementioned data are presented in table 4. It is worth noting that both approaches provide the correct qualitative description of the experimental findings, where the highest blue- and red-shift is observed for (**1**) and (**4**), respectively. Nevertheless, the linear response solvation gives a rather poor, quantitative description of the emission wavelengths. When state-specific solvation is taken into account a significant improvement is observed accompanied by a hypsochromic shift of the theoretical data towards the experimental values. Even though, the aforementioned approach does not fully match the observed wavelengths there is a constant difference of *ca*. 80 nm in comparison to the experiment.

What is also interesting, upon re-optimizing geometries in the search for the excited states the planarization of the structure of each molecule is observed, which is evidenced by the dihedral angles between adjacent rings approaching zero (see Table SI.2. - Supporting Information). This observation supports the analysis of emission spectra of compounds (**1**) through (**4**) presented above.

Table 4 - Emission wavelengths and energies computed via linear response- and state-specific solvation reaction field at B3LYP/6-31g(d,p) level of theory.

Code	λ_{em} – linear response (nm)	Emission energy – linear response (eV)	λ_{em} – state specific solvation (nm)	Emission energy - state specific solvation (eV)
1	551.39	2.25	501.19	2.47
2	598.57	2.07	537.18	2.31
3	570.81	2.17	519.43	2.39
4	618.77	2.00	561.04	2.21

3.2. Redox properties of monomers: theory *versus* experiment

Detailed knowledge of the redox properties of new organic semiconductors does not only shine light on their physical chemistry but also is crucial for any attempt of their application in the fabrication of electronic, optoelectronic or electrochemical devices. In this respect, cyclic voltammetry investigations are complementary to the spectroscopic ones since they give access to the determination of the ionization potential (IP) and electron affinity (EA) which are closely related to the positions of the HOMO and LUMO levels.

IP can be calculated from the formal potential of the first redox couple corresponding to the oxidation of the neutral molecule to a radical cation whereas EA from the formal potential of the couple associated with the reduction of the neutral molecule to a radical anion. Four molecules described in this paper undergo both electrochemical oxidation and electrochemical reduction, albeit of irreversible nature (**Figure 2**). The irreversibility of oxidation is caused by the consecutive radical cations coupling, resulting in electropolymerization. The electropolymerization product gives rise to a reduction peak in the reverse scan of the cyclic voltammogram (**Figure 2**).
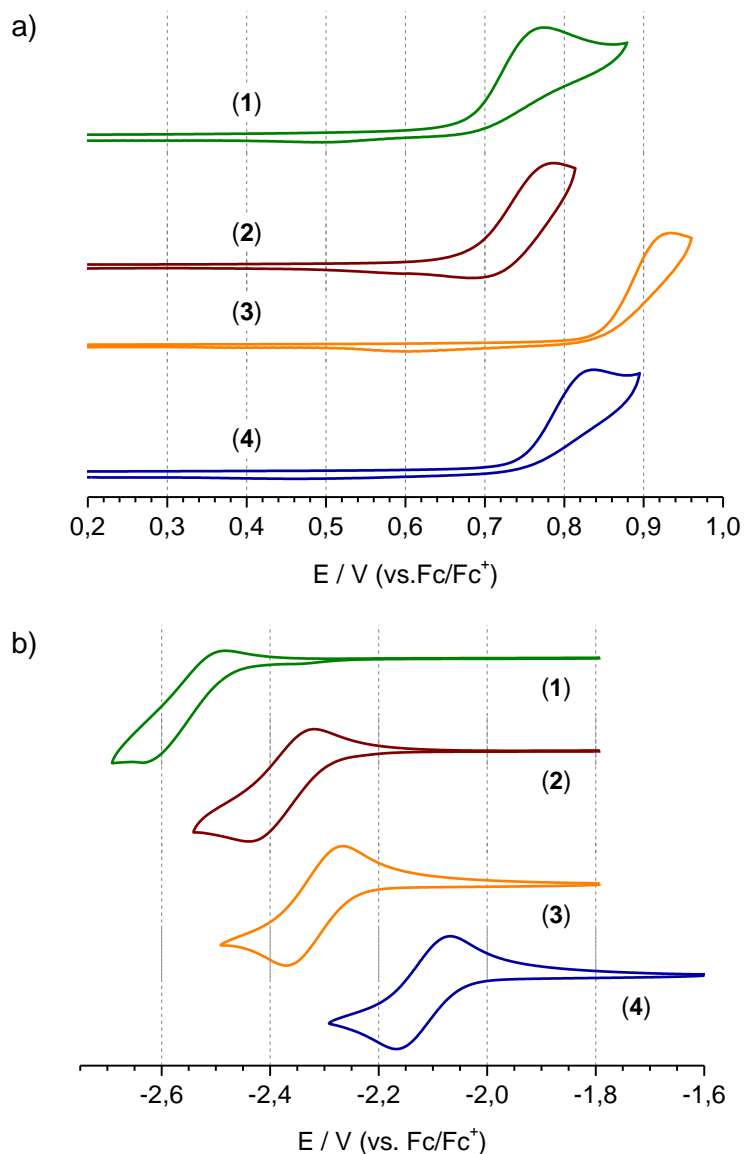
Figure 2 - Cyclic voltammograms of compounds 1, 2, 3 and 4, registered in : **a)** 0.1M Bu$_4$NPF$_6$ in dichloromethane for the anodic potential ranges, and **b)** in 0.1M Bu$_4$NPF$_6$ in tetrahydrofuran for the cathodic potentials range. Scan rate: 100 mV/s.

In the case of irreversible redox processes, the onsets of the oxidation and reduction peaks are taken for the calculation of IP and EA, instead of the formal potentials (see figures SI.2 and SI.3) despite the fact that all four structures feature reasonably reversible electrochemical reduction (figure 2) This approach is necessary to permit direct comparison of the derived values. It should

be noted here that the values obtained from the oxidation peak onsets correlate well with the IP values derived from photoelectron spectroscopy, which is a direct method of IP determination.[54] The electrochemically determined IP and EA values are listed in Table 5. It is instructive to compare the potentials of the oxidation and reduction onsets for compounds (**3**) and (**4**) (Figure 2). (**4**) is easier to oxidize and by consequence exhibits a lower IP value by about 0.10 eV compared to (**3**). The presence of oxadiazole unit in monomer backbone probably has a stronger influence on lowering the π-electron density in the adjacent thiophene rings and makes the formation of the radical cation more difficult [26], however this result is somewhat inconsistent with stronger electron withdrawing properties of the thiadiazole ring whose LUMO level computes to -1.76 eV (calculated using DFT/B3LYP/6-31G(d)/DCM functional set) compared to the oxazole one, being equal to -0.48V. Stronger aromaticity of thiadiazole may be the crucial factor here. Aromatic stabilization energy for thiadiazole ring is 13.69 whereas for oxadiazole 7.78. [48,49] Higher aromaticity of the thadiazole ring compared to the oxadiazole one is also evidenced by the calculations of their harmonic oscillator measure of aromaticity (HOMA) indices. [49,55] This apparently promotes improved electron communication between the two bithiophene pendants in (**4**), hence lowering the oxidation potential of this pentaring entity. Compound (**4**) turns out easier to reduce as well, showing a larger (EA) value than (**3**) (Table 3). This observation is in turn consistent with the stronger electron accepting character of thiadiazole rationalizing the sizeable – ca. 0.3V difference of reduction potentials of (**3**) and (**4**) These results follow the trends observed for spectroscopic π-π* transition energy values, showing that simple evaluation of spectral data may be insufficient to expressly compare different donor-acceptor systems. Replacing alkyl substituents with alkoxy ones in oxadiazole derivatives facilitates oxidation of compound (**2**) and makes its reduction more difficult, consistent with stronger electron donating properties of the alkoxy group. Oxidation potential of (**2**) is lower than (**3**) by

about 0.20 V (Figure 2) which also confirms stronger electron donating character of the alkoxy side chain. The difference in electron affinity of both compared compounds (**2**) and (**3**) is insignificant (0.06 eV). This phenomenon suggests that the kind of side chain (alkoxy or alkyl) has little influence on the reduction ability of examined compounds.[26] Triazole ring in (**1**) has stronger electron donating properties than the oxa- and thiadiazole ones. As a result, it is easy to oxidize (comparable only to (**2**)) and the most difficult to reduce, showing the lowest value of EA. Finally, it should be stated that the ΔE values, calculated from the potentials of the onsets of the reduction and oxidation peaks follow the same trend as the optical ones, being consistently slightly larger (compare data in Table 2 and Table 5).

The theoretically predicted energies of the HOMO and LUMO levels are listed in Table 6 whereas the frontiers orbitals are depicted in Figure 3. For comparison, data for compound (**5**) are also included. As typical for oligothiophenes and similar D-A-D molecules, both HOMO and LUMO are well delocalized throughout the molecule backbone.[56,57] In order to account for the dynamics of electrochemical processes and geometry changes which accompany them, IP and EA were calculated theoretically. Usually, the introduced level of theory is appropriate in case of poly- and oligothiophenes[56–59], yielding almost a perfect match between the theory and experiment, however herein some exceptions were found. Qualitatively, the theoretical values of IP and EA follow the pattern of the electrochemical data with IP rising in the series (**2**), (**1**), (**4**), (**3**) and EA from (**1**) to (**4**). By comparing the values with the aim of getting quantitative relationships, one can easily find that both theoretical IP and EA are overestimated by ca. 0.6-0.7 eV. This effect is systematic and can be attributed to the mathematical expression of the functional.

HOMO   **LUMO**
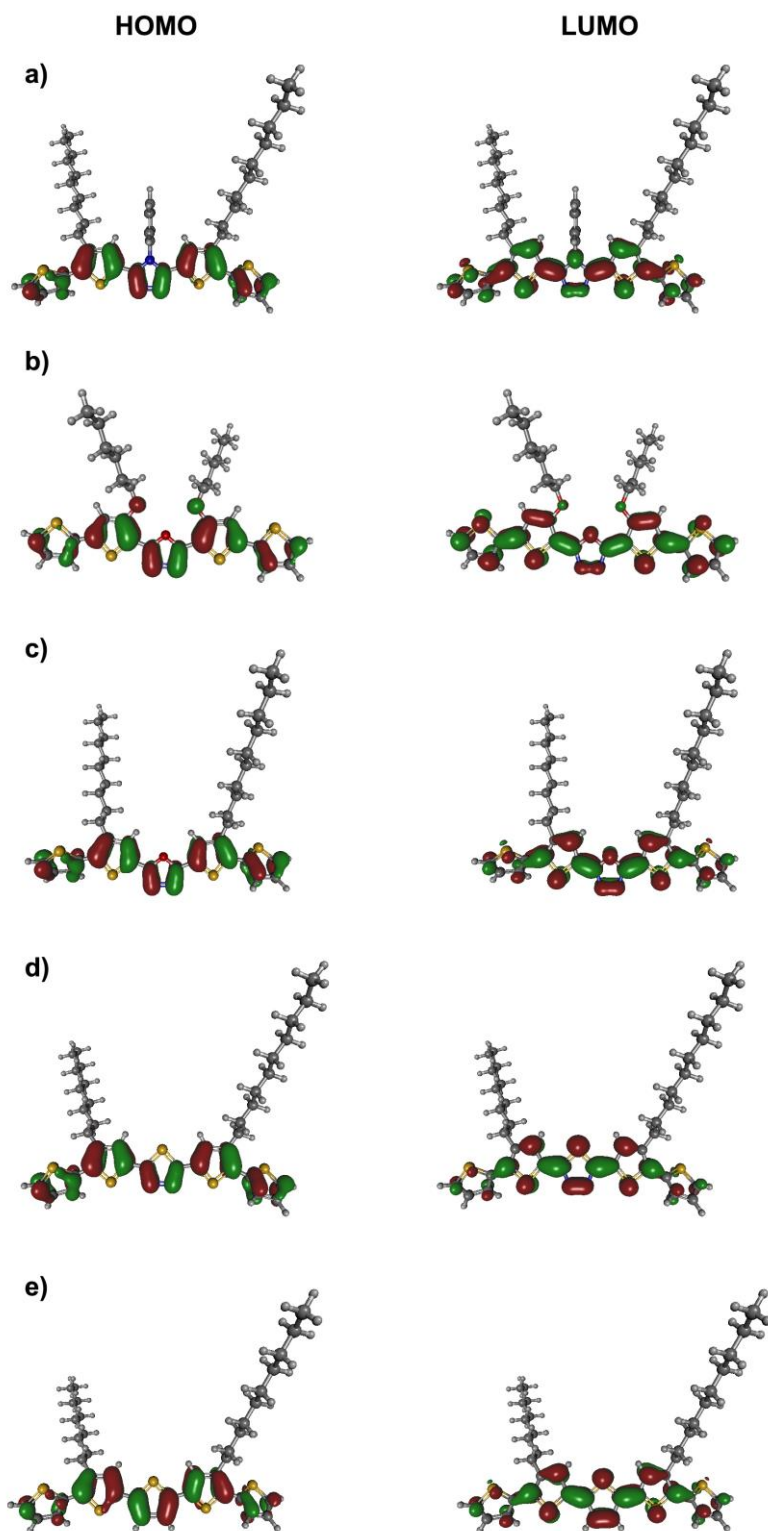
Figure 3 - Frontier molecular orbital plots (isovalue=0.03 green for positive and red for negative sign) for molecules **a**) 1, **b**) 2, **c**) 3, **d**) 4 **e**) 5**.**

Table 5 - IP and EA values electrochemically determined from the redox potentials for the penta-ring compounds studied (1-4)

Compound	E^{ox}_{onset} [V]	E^{red}_{onset} [V]	IP[a] [eV]	EA[b] [eV]	ΔE [eV]
1	+0.66	-2.46	5.76	2.64	3.12
2	+0.63	-2.28	5.73	2.81	2.91
3	+0.83	-2.23	5.93	2.87	3.06
4	+0.73	-2.04	5.83	3.06	2.77

[a] calculated according to equation $IP(eV) = |e|(E_{ox, onset} +5.1)$
[b] calculated according to equation $EA(eV) = |e|(E_{red, onset} +5.1)$

Table 6 - Theoretically predicted HOMO, LUMO IP and EA energies for the penta-ring compounds studied (B3LYP/6-31G(d,p) level of theory). Calculations for compound (5) are presented for comparison.

| Compound	Environment	HOMO [eV]	LUMO [eV]	ΔE [eV]	IP [eV]	EA [eV]
1	Vacuum	-5.15	-1.60	3.54	6.37	0.39
	CH_2Cl_2	-5.36	-1.80	3.56	5.09	2.06
2	Vacuum	-4.93	-1.84	3.09	5.87	0.88
	CH_2Cl_2	-5.16	-2.06	3.10	5.00	2.18
3	Vacuum	-5.45	-1.96	3.50	6.26	1.07
	CH_2Cl_2	-5.56	-2.11	3.47	5.29	2.33
4	Vacuum	-5.39	-2.17	3.22	6.17	1.24
	CH_2Cl_2	-5.51	-2.33	3.18	5.21	2.54
5	Vacuum	-4.92	-1.84	3.08	5.76	1.02
	CH_2Cl_2	-5.03	-2.00	3.03	4.78	2.26

3.2 Electropolymerization and redox properties of the polymerization products

All investigated penta-ring compounds are thienyl ring-capped with unblocked C_α positions. Upon electrochemical oxidation, all of them electropolymerize readily. The process can be carried out using cyclic voltammetry (CV)[23] where the reaction progress can be precisely

controlled through the number of consecutive scans. A representative set of cyclic voltammograms, featuring the electropolymerization of compounds (**1**) through (**4**) is shown in Figure 4. One should note here that electropolymerization of monomers containing strongly electron accepting central group connected to thiophene moiety is difficult and does not occur in three-ring compounds because of the high potential of the radical cation formation and its instability.[24] However, five-ring compounds studied herein, readily electropolymerize, contrary to compound (**5**) which, as a quinquethiophene, is known to feature a two-step reversible redox electrochemistry with negligible signs of dimerization. Such behavior of compounds (**1**) through (**4**) indicates that the central, electron accepting heterocycle acts as a conjugation attenuator, effectively making the investigated compounds behave more like shorter oligothiophenes. Taking into account the fact that the longest dimerizing oligothiophene radical cation is a quaterthiophene one, this implies that each investigated molecule behaves as two fused shorter oligothiophenes, ter- or quater- ones, explaining their observed polymerization propensity.

Upon electrochemical oxidation, polymerization of donor-acceptor moieties is often observed.[60,61] It is known that electron donating groups in the 3-position of thiophene decrease the oxidation potential of the monomer and increase the stability of its cation radical.[62] The main reason for this effect is that the HOMO level of investigated monomers lies higher compared to non-substituted oligothiophenes, making the incipient radical cations more reactive, giving the time necessary for the coupling steps to take place which leads to formation of higher molecular mass products.[62] All examined compounds polymerize readily at relatively low oxidation potentials. Compound (**3**) undergoes polymerization most easily, already at potentials of the onset of its first oxidation peak at ca. +0.87 V (Figure 4c), In all four cases, irreversible oxidation of the monomers result in the formation of radical cations which consecutively undergo rapid intermolecular C_α-C'_α coupling, yielding the polymerization product. For (**3**) and (**4**), beginning

from the second cycle, two clearly-defined redox couples can be distinguished, gradually growing in intensity upon consecutive cycling (figures 4c and 4d). In principle, these clear steps can be associated with successive redox transformations of the conjugated macromolecular chains, the first one representing oxidative generation of radical cations, while the second one signaling their transformation to spinless dicationic species. The technicalities of these compound individual transitions will be elaborated further when the results of coupled UV-Vis-NIR-EPR spectroelectrochemical measurements will be discussed. The fact that singular redox steps can be picked out on the voltammograms of electrosynthesized polymers suggests that a limited polymerization degree has been attained. This observation comports with our previous findings for similar, though soluble electropolymerized compounds, whereby SEC chromatography showed that dimers, trimers and tetramers dominated the products of electropolymerization.[24]
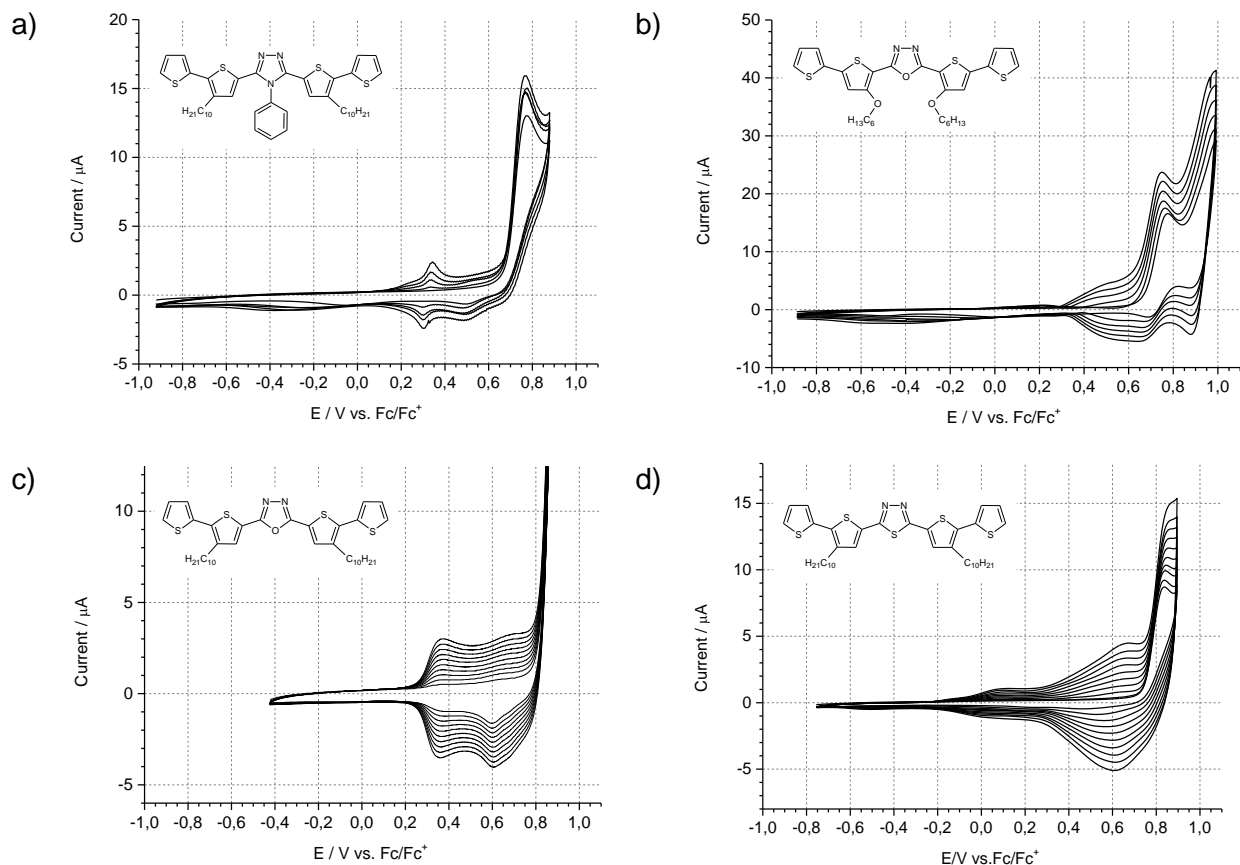
Figure 4 - Cyclic voltammograms of anodic oxidation of **a**) 1, **b**) 2, **c**) 3 and **d**) 4 at platinum electrode in 0.1M Bu$_4$NPF$_6$ in dichloromethane at a scan rate of 100 mV/s, showing successive accumulation of an electroactive deposits in the course of repetitive potential cycling.

In their cyclic voltammograms, registered in the positive potential range (Figure 5a), all four polymerization products studied show two, more or less overlapping redox couples. In the negative potentials range a reduction process occurs which is only partially reversible for the poly(**2**), poly(**3**) and poly(**4**) and irreversible for the triazole derivative (poly(**1**)). Cyclic voltammograms showing individual p-doping and n-doping onsets are presented in Figure SI.4 and Figure SI.5 of Supporting Information. Obtained polymerization products (poly1-4) show highly reversible electrochemical couples upon p-doping process, especially the first ones, albeit poly(**1**) and poly(**2**) in quite limited potential ranges. The potential shift values of the first peak -

$\Delta E = E_{ox}-E_{red}$ are close to 0.20 V and 0.30 V for poly(**3**) and poly(**4**), while poly(**1**) is characterized by the smallest difference between the p-doped and de-doped peaks of about 0.03 V, indicating surface bound electroactive species undergoing Nernstian controlled electron exchange. This high electrochemical reversibility is observed for the singly oxidized state, which may as well suggest that the positive charge is strongly localized, with polaronic state extending over a very short conjugated segment of the polymer chain.[63] That observation finds further backing in decently localized and well-defined absorption peaks of the oxidized films, developing in the Visible and NIR regions (*vide infra*).[62]
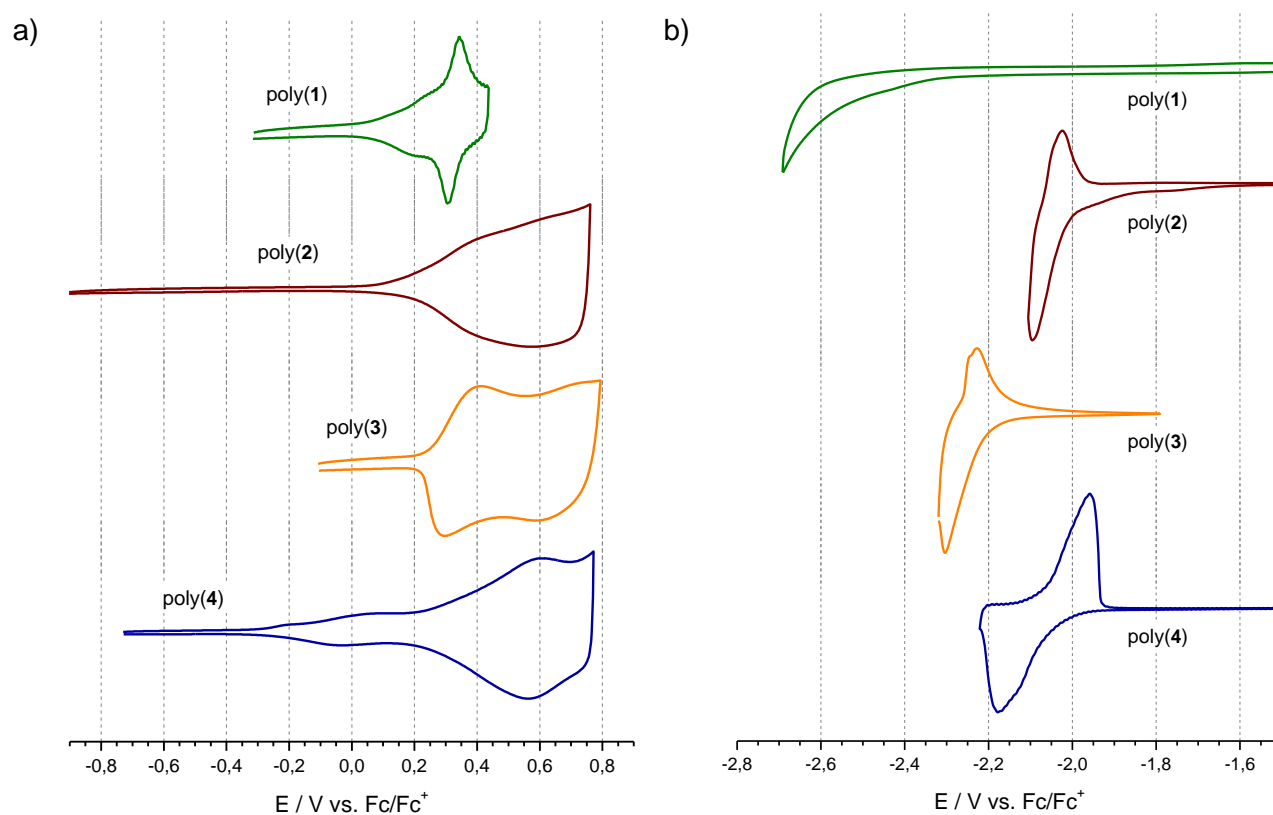
Figure 5 - Cyclic voltammograms of electrochemically deposited poly(1), poly(2), poly(3) and poly(4) at platinum electrode registered in: **a**) 0.1M Bu$_4$NPF$_6$ in dichloromethane for the anodic potential range, **b**) 0.1M Bu$_4$NPF$_6$ in tetrahydrofuran for the cathodic potential range. Scan rate: 100 mV/s.

Analyzing the cathodic potential range voltammograms of poly(**1**) through poly(**4**) (figure 5b) we can see that, save poly(**1**) which does not seem to reduce in the available working potential range of the electrolyte, all the other three polymers undergo moderately reversible reduction between -2.0 V and -2.3 V. This indicates that the electrophilicity and conjugation transmission factors of the electron accepting heterocycles balance out, yielding extended π-conjugated segments of comparable electron affinity. Upon repetitive potential cycling in carefully deaerated anhydrous electrophobic electrolyte, the polymer's radical anion redox pair is quite stable, enduring tens of cycles at scanning speeds of 0.1 V/s. An interesting, common trait of poly(**2**) and poly(**3**) responses is the sharpness of their radical anion redox pair. Such narrow potential range response points to potential defined redox process which in turn translates to clear localization of the anion charge on the redox active molecule. Given the fact that oligo and polythiophenes preferably get p-doped [64–66] than n-doped [67], the only possible site for the localization of the negative charge is the heterocylce ring itself. [68] Such charge concentration may draw deleterious consequences regarding the stability of the n-doped state of the polymer, however, hinted by the complex CV trace of the reduction of poly(**4**), whose asymmetric, 0.2 V separated reduction and reverse oxidation peaks indicate complex electrochemical – chemical behavior of the nascent polymeric radical anion. The shape and separation of the CV peaks points to some chemical transformation of the radical anion to an electroactive structure, prevalent enough to undergo oxidation to original undoped polymer chain in the reverse cathodic potential run.

Table 7 gathers the electrochemical data describing redox properties of the obtained polymers. They are compared with those coming from the PBC-DFT calculations (Table 8).

Table 7 - IP and EA values electrochemically determined (from the redox potentials) for electrochemically polymerized penta-ring compounds.

Compound	E_g^{ec} [eV]	E^{ox}_{onset} [V]	E^{red}_{onset} [V]	IP [eV]	EA [eV]	E_g^{opt} [eV]
poly(1)	2.37	+0.06	-2.31	5.16	2.79	2.23
poly(2)	2.15	+0.13	-2.02	5.23	3.08	2.05
poly(3)	2.44	+0.23	-2.21	5.33	2.89	2.11
poly(4)	1.76	-0.29	-2.05	4.81	3.05	1.89

**Table 8** - PBC/B3LYP/6-31G(d,p) calculations for polymers corresponding to the studied monomers.

Compound	HOCO [eV]	LUCO [eV]	Eg [eV]
poly(1)	-4.78	-2.13	2.64
poly(2)	-4.73	-2.48	2.25
poly(3)	-5.05	-2.52	2.53
poly(4)	-4.97	-2.60	2.37
poly(5)	-4.63	-2.30	2.33

A comparison of the data presented in Tables 5 and 7 unequivocally shows that the extension of the conjugation due to electropolymerization mainly effects the IP value, the EA values remaining very close to those determined for the monomer. The most pronounced decrease of IP is observed for poly(**4**) consistent with better aromaticity of the thiadiazole ring and better conjugation of the resulting polymer**s**. For the alkyl substituted compounds, the trend found in the monomers is reproduced in the polymer**s**.

The effect of the nature of the solubilising substituent is different. Replacement of an alkyl group by a more electrodonating alkoxy one results in a relatively large decrease of |EA|, as

expected. At the same time, lowering of IP caused by the extension of the conjugation is less pronounced than in the alkyl-substituted analogue.

Table 8 gathers the energies of crystal orbitals obtained *via* PBC-DFT calculations, which were carried out on optimized unit cells composed of two molecules of each of the four compounds studied. The results for quinquethiophene derivative were again added here as a reference. The optimized unit cell for poly(**4**) is presented in figure 6 as an example, whereas the remaining polymer unit cells are presented in supporting information (Figure SI.9). What is interesting to note is that the backbone of the polymer is bent along translational vector forming an S-type structure, which can be best seen in the top view (fig. 6). In this case, the HOCO and LUCO values correspond to what can be derived from cyclic voltammetry as IP and EA, respectively. As anticipated, a simultaneous rise in the HOCO and lowering of LUCO compared to HOMO and LUMO of the corresponding compounds (**1**)-(**4**) is observed. As a consequence, also the E_g value for the polymers is significantly lowered. There is, however, a difference in the way these values change when moving from monomers to polymers. The lowest value of HOCO was found in the case of poly(**3**) (-5.05 eV) and the highest for poly(**2**). At the same time LUCO values were the lowest for poly(**4**) and the highest for poly(**1**).
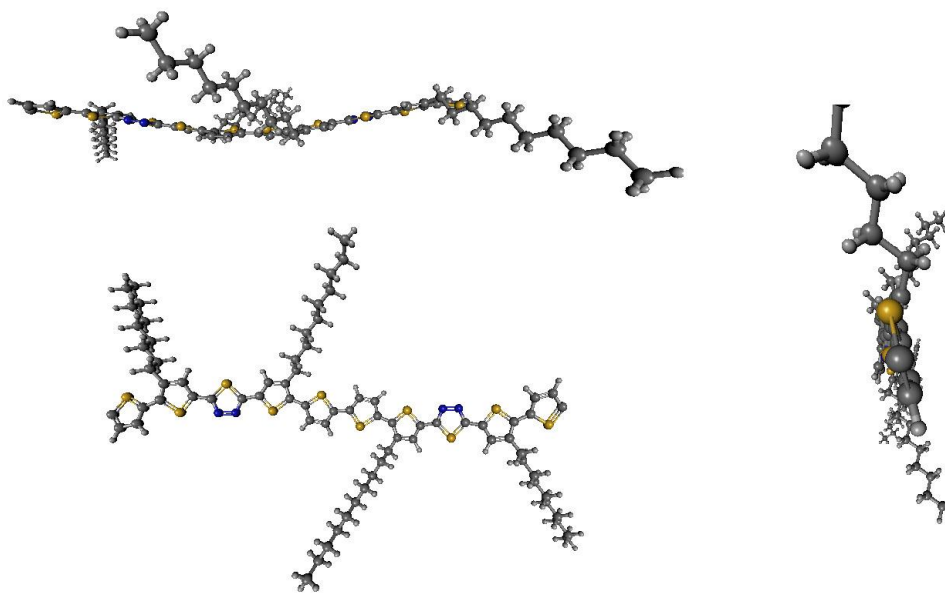
Figure 6 - Projections of a unit cell optimized for polymer corresponding to compound 4 at PBC/B3LYP/6-31G(d,p) level of theory, along: top, side and translational vector view.

3.3 UV-Vis-NIR and EPR spectroelectrochemistry of the electropolymerized compounds

Cyclic voltammetry investigations are phenomenological in nature, therefore it is instructive to support them with spectroelectrochemistry. Oxidation of conjugated polymers gives rise to pronounced spectral changes in the visible and NIR part of the spectrum, which can be correlated with the formation radical cations and consecutively, spinless diactions, whose presence introduces domains of polaronic and bipolaronic nature to the polymer chains.[69–72] This process is commonly called p-type doping. By analogy, the formation of negative polarons and bipolarons in the process of neutral polymer chain reduction is termed n-type doping. In particular, the formation of polarons gives rise to two doping-induced transitions whereas one transition of this type is characteristic for bipolarons.[73–76] Moreover polarons carry unpaired spins, thus their formation and recombination to bipolarons can be monitored by EPR spectroscopy.[77–80]

Spectroscopic parameters of the investigated polymers in the neutral and p-doped states are collected in Table 9. With the exception of poly(**4**), in the spectra of thin films of neutral polymers a clear vibrational structure can be seen, which is the most pronounced in poly(**3**). This finding can be considered as a manifestation of higher chain stiffness of poly(**3**), compared to other investigated layers. We have deconvoluted the spectra of each deposited polymer film. It was found that a set of five Voigt functions of increasing width superimposed on a fixed baseline can successfully simulate the spectra in each case (see fig. SI.6 and table SI.3). The differences between the maxima of the first two deconvoluted peaks are in range of ca. 1330 – 1450 cm^{-1}, which nicely corresponds to strong vibrational absorption observed for oligothiophenes in their FT-IR and Raman spectra.[81–83]

Table 9 - Electronic transitions in electrochemically polymerized penta-ring compounds in their neutral and oxidized states. Energies of polaronic and bipolaronic transitions are given for highest applied potential.

Compound	λ_{max} of the π-π* $S_0^{v=0} \rightarrow S_1^{v}$ transitions of the neutral polymer [eV]					E_g^{opt} [eV]	λ_{max} of the polaron bands [eV]	λ_{max} of bipolaronic band (est.) [eV]
	v = 0	v = 1	v = 2	v = 3	v = 4			
poly(1)	2.37	2.55	2.76	2.99	3.43	2.23	1.78; 0.89	1.49
poly(2)	2.23	2.39	2.56	2.82	3.36	2.05	1.79; 0.72	1.50
poly(3)	2.26	2.44	2.66	2.87	3.20	2.11	1.83; 1.00	1.55
poly(4)	2.05	2.21	2.41	2.63	3.01	1.89	1.74; 0.95	1.44

The optical band gaps, determined from the onset of the *0-0* transition within the π-π* vibronic band follow the trend found for the electrochemical band gaps, being however slightly lower (compare Tables 3 and 7).

For UV-Vis-NIR spectroelectrochemical experiments, thin, optical quality polymeric films were deposited on an ITO electrode and their spectra were recorded for increasing electrode potentials (p-doping mode), covering the potentials of the first and the second redox couples of the cyclic voltammogram. In Figure 7 the spectral response of each film to the increasing electrode polarization is shown (see also figure SI.7 for spectra of poly(**2**) in a broader wavelength range). The first spectral changes induced by the oxidation appear at potential coinciding with the onset of the first anodic peak in the cyclic voltammogram. In the potential range covering the first redox couple three transitions can be distinguished (the two higher energy ones overlap strongly) which grow in intensity with increasing potential. As already said, two doping-induced transitions originate from the presence of polarons, while only one comes from bipolarons. It can therefore be concluded that at these intermediate potentials, polarons are present, possibly coexisting with a small amount of bipolarons. At the end of the oxidative doping only two doping-induced bands can be seen, probably due to masking of weak bipolaron band by higher energy polaron ones, suggesting that polarons are the dominant, electrochemically generated charge carriers in those materials. It can therefore be postulated that polarons reside on the quatertiophene segments of the polymer, for which the azole moieties constitute a certain conjugation interrupt, hindering the formation of bipolarons usually stabilized at longer oligotiophene chains[72,73].

All spectroelectrochemical data are collected in Table 9. One should notice differences in the energies of the doping-induced bands in the studied polymers. A comparison of these bands in poly(**3**) and poly(**4**) again indicates better conjugation between the thadiazole ring and quatertiophene than for the oxadiazole analogue, brought about by higher aromaticity of thiadiazole. The replacement of an alkyl substituent by an alkoxy one results in an increase of the

bipolaronic bands separation caused by a significant bathochromic shift of the less energetic band.
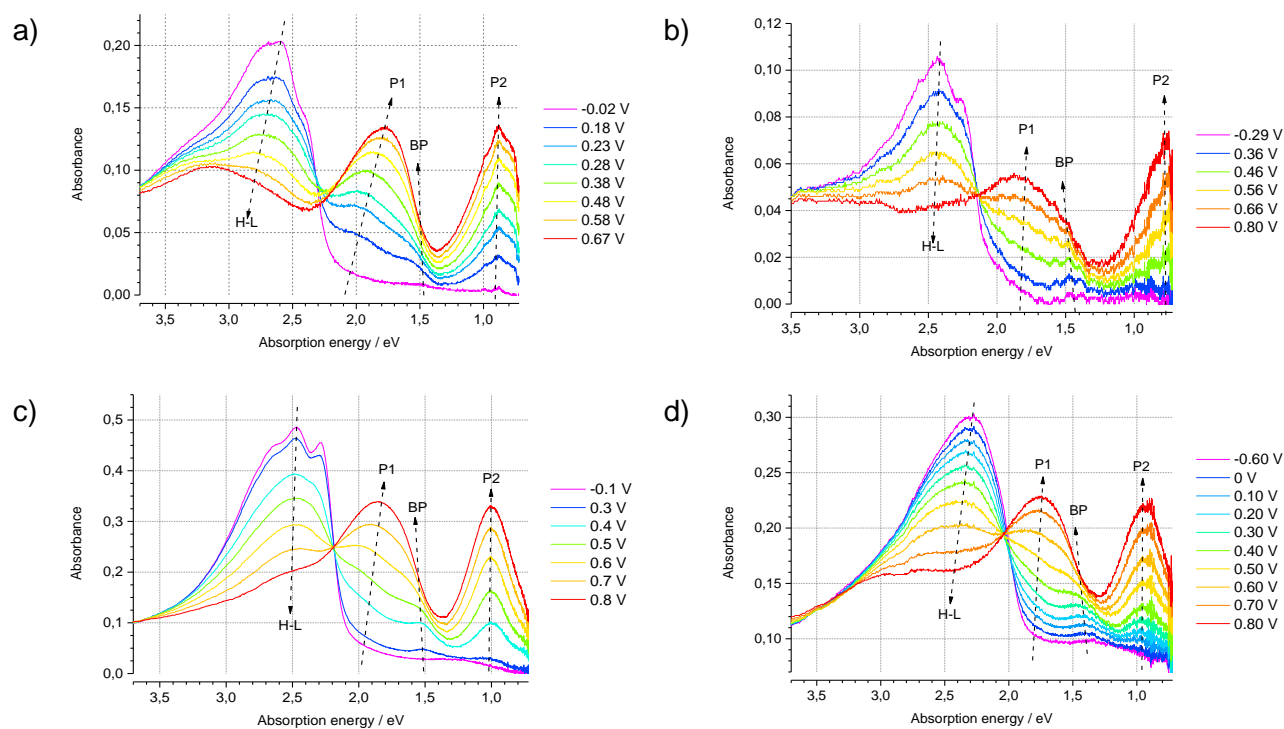
Figure 7 - UV-Vis-NIR spectra of thin layers of: **a**) poly(1); **b**) poly(2); **c**) poly(3); **d**) poly(4) registered for increasing electrode potentials. E vs Fc/Fc$^+$. Abbreviations used: H-L – HOMO to LUMO transition, P1 – first polaronic transition, P2 – second polaronic transition, BP – bipolaronic transition.

As already stated, the formation of polarons and their recombination to bipolarons can be investigated in EPR spectroelectrochemical experiments showing the relative changes in the spin concentration as a function of the working electrode potential. In Figure 8 the concentration of paramagnetic species is plotted as a function of the working electrode potential, together with the cyclic voltammograms, which are shown for comparison. This concentration can be considered proportional to the number of paramagnetic species, hence polarons.
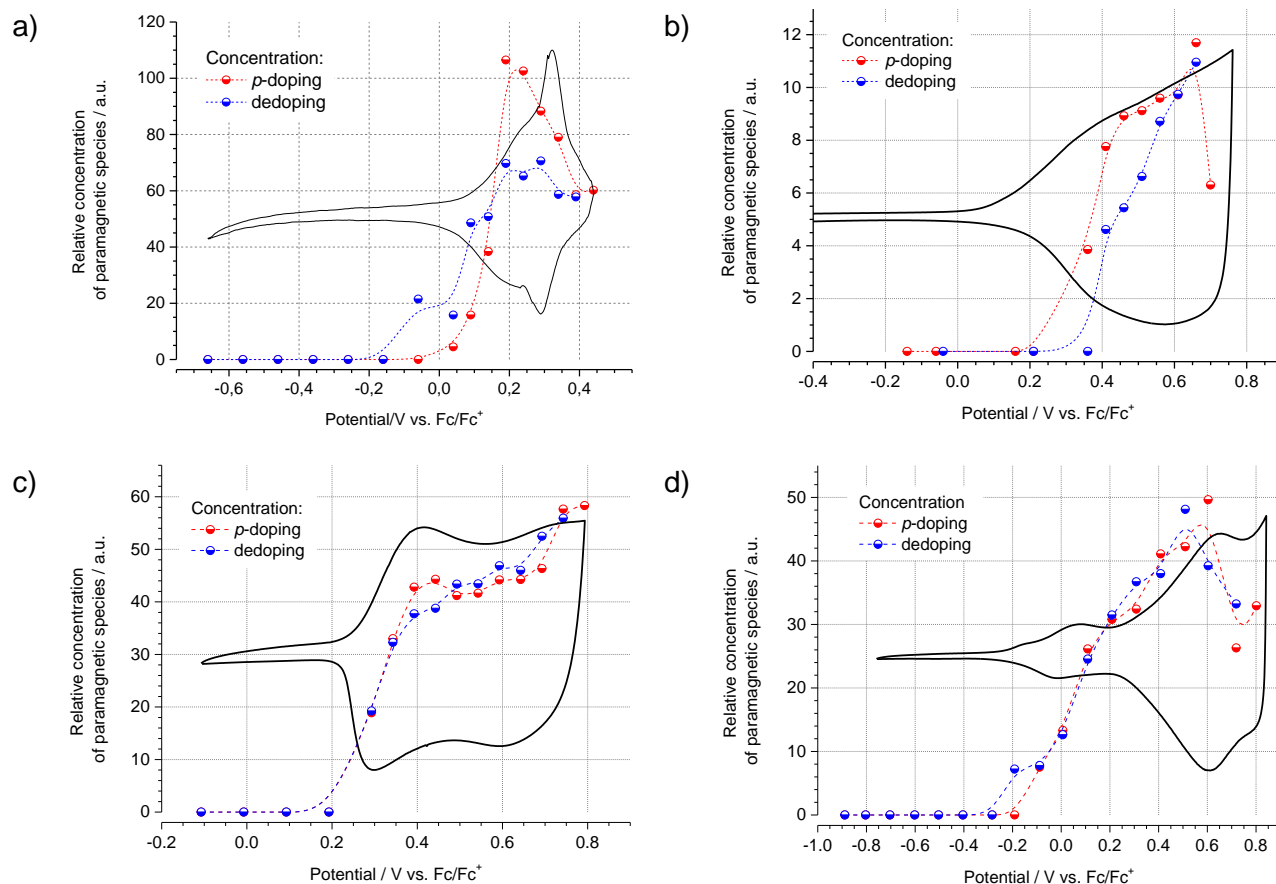
Figure 8 - Relative concentration of unpaired spins in thin films of a) poly(1); b) poly(2) c) poly(3); d) poly(4), as a function of the working electrode potential during doping and subsequent dedoping. The corresponding cyclic voltammograms of polymer thin films are shown for reference.

Poly(**1**) and poly(**2**) yielded very weak signals (see figure SI.8), which could be attributed to formation of bipolarons right from the beginning of the doping process. There is, however, little support for this inference in the UV-Vis-NIR spectroelectrochemical data, discussed earlier. Low concentration of polarons in those examples is probably connected with electropolymerization process. In case of poly(**1**) only small amount of film is created on the electrode, which is probably responsible for the observed weak signals. In case of poly(**2**) polymerization occurs only after the second oxidation peak of the monomer is reached. This

probably leads to defected polymeric layers with poor doping abilities, which resulted in low intensity of EPR signals.

In the case of poly(**3**) unpaired spins appear at the potential coinciding with the onset of the first oxidation peak and then their concentration increases up to the upper potential limit of the doping experiment. This indicates that polarons are created throughout the entire doping process, which conforms to the UV-Vis-NIR spectroelectrochemical results discussed earlier. Electrochemical doping of poly(**4**) proceeds in a similar manner, with steady growth of spin concentration from the beginning of the doping process till the potential of the second voltammetric redox peak. Differences however occur when the potential of third CV peak of poly(**4**) is applied, whereby a decrease of the number of unpaired spin is observed, ascribable to the formation of spinless bipolarons. The differences between poly(**3**) and poly(**4**) can be again attributed to higher conjugation of thiadiazole ring with quarterthiophene moieties, compared to the oxadiazole ring, stabilizing the formation of bipolarons at high doping levels. As can be seen in (figure 8d), however, even at the highest doping levels one can observe a high spin concentration in poly(**4**). In contrast to poly(**1**) and poly(**2**), the dedoping process of poly(**3**) and poly(**4**) proceeds along an almost reverse path to that of doping, which highlights good thermodynamic reversibility of the doping process of these polymeric materials. A somehow weaker point of the EPR spectroscopy here, is that it does not detect the presence of spinless bipolarons. Therefore no conclusions can be drawn concerning the relative populations of the two coexisting charge storage configurations (polarons and bipolarons). However, by correlating the data of UV-Vis-NIR and EPR spectroelectrochemistry it can be postulated that polarons dominate the doping process of investigated polymers.

4. Conclusions

To summarize, we have demonstrated that penta-ring compounds consisting of an electroaccepting central ring such as 1,3,4-oxadiazole, 1,3,4 - thiadiazole or 1,2,4-triazole, symmetrically connected to substituted bithiophene constitute an interesting class of solution processable electroactive and luminescent semiconductors. Their HOMO and LUMO levels and, by consequence, the values of IP and EA can be conveniently tuned either by changing the nature of the central ring or by replacing alkyl solubilizing substituents by alkoxy ones, which lower the IP and |EA| values All four compounds can be used as monomers for oxidative electrochemical polymerization. For the derivatives with alkyl substituents, electropolymerization mainly affects their IP, whose values are significantly reduced compared to the corresponding monomers, whereas EA values remain essentially unchanged. In the alkoxy derivative both IP and EA are modified upon electropolymerization. The electropolymerization products show an excellent electrochemical reversibility in their oxidative doping process as demonstrated by cyclic voltammetry, UV-Vis-NIR and EPR spectroelectrochemistry. The studied monomers and polymers are promising candidates for the fabrication of organic opto-electronic devices and preliminary studies show that the former can be used as luminophores in host-guest type light emitting diodes.

5. Acknowledgments

Supporting Information include: deconvoluted fluorescence spectra and tabulation of spectral parameters together with dihedral angles in ground and excited state of compound 1 through 4 molecules, deconvoluted UV-Vis spectra and tabulation of spectral parameters of undoped poly(**1**) through poly(**4**), clean platinum electrode cyclic voltammograms of compounds 1 through 4 and their electropolymers, used to determine their ionisation potentials and electron affinities, broad spectral range, doping dependent ensemble of UV-Vis-NIR spectra of poly(**2**) featuring its lowest energy transitions , EPR lines of poly(**1**) through poly(**4**) at different doping potentials, and computationally optimized projections of unit cells of poly(**1**) through poly(**4**). This material is available free of charge via the Internet at http://pubs.acs.org

6. References

(1)   Balan, A.; Gunbas, G.; Durmus, A.; Toppare, L. Donor−Acceptor Polymer with Benzotriazole Moiety: Enhancing the Electrochromic Properties of the "Donor Unit." *Chem. Mater.* **2008**, *20*, 7510–7513.

(2)   Ellinger, S.; Graham, K. R.; Shi, P.; Farley, R. T.; Steckler, T. T.; Brookins, R. N.; Taranekar, P.; Mei, J.; Padilha, L. A.; Ensley, T. R.; et al. Donor–Acceptor–Donor-Based Π-Conjugated Oligomers for Nonlinear Optics and Near-IR Emission. *Chem. Mater.* **2011**, *23*, 3805–3817.

(3)   Hains, A. W.; Liang, Z.; Woodhouse, M. A.; Gregg, B. A. Molecular Semiconductors in Organic Photovoltaic Cells. *Chem. Rev.* **2010**, *110*, 6689–6735.

(4)   Bujak, P.; Kulszewicz-Bajer, I.; Zagorska, M.; Maurel, V.; Wielgus, I.; Pron, A. Polymers for Electronics and Spintronics. *Chem. Soc. Rev.* **2013**, *42*, 8895–8999.

(5)   Cheng, Y.-J.; Yang, S.-H.; Hsu, C.-S. Synthesis of Conjugated Polymers for Organic Solar Cell Applications. *Chem. Rev.* **2009**, *109*, 5868–5923.

(6)   Wang, C.; Dong, H.; Hu, W.; Liu, Y.; Zhu, D. Semiconducting Π-Conjugated Systems in Field-Effect Transistors: A Material Odyssey of Organic Electronics. *Chem. Rev.* **2012**, *112*, 2208–2267.

(7)   Pron, A.; Gawrys, P.; Zagorska, M.; Djurado, D.; Demadrille, R. Electroactive Materials for Organic Electronics: Preparation Strategies, Structural Aspects and Characterization Techniques. *Chem. Soc. Rev.* **2010**, *39*, 2577–2632.

(8)   Wu, W.; Liu, Y.; Zhu, D. Pi-Conjugated Molecules with Fused Rings for Organic Field-Effect Transistors: Design, Synthesis and Applications. *Chem. Soc. Rev.* **2010**, *39*, 1489–1502.

(9)   Xiang, H.; Cheng, J.; Ma, X.; Zhou, X.; Chruma, J. J. Near-Infrared Phosphorescence: Materials and Applications. *Chem. Soc. Rev.* **2013**, *42*, 6128–6185.

(10)   Lange, U.; Roznyatovskaya, N. V; Mirsky, V. M. Conducting Polymers in Chemical Sensors and Arrays. *Anal. Chim. Acta* **2008**, *614*, 1–26.

(11)   Zhao, Y.; Guo, Y.; Liu, Y. 25th Anniversary Article: Recent Advances in N-Type and Ambipolar Organic Field-Effect Transistors. *Adv. Mater.* **2013**, *25*, 5372–5391.

(12)   Van Mullekom, H. Developments in the Chemistry and Band Gap Engineering of Donor–acceptor Substituted Conjugated Polymers. *Mater. Sci. Eng. R Reports* **2001**, *32*, 1–40.

(13)   Tarkuc, S.; Udum, Y. A.; Toppare, L. Tailoring the Optoelectronic Properties of Donor–acceptor–donor Type Π-Conjugated Polymers via Incorporating Different Electron-Acceptor Moieties. *Thin Solid Films* **2012**, *520*, 2960–2965.

(14)   Liu, B.; Yu, W.-L.; Lai, Y.-H.; Huang, W. Blue-Light-Emitting Fluorene-Based Polymers with Tunable Electronic Properties. *Chem. Mater.* **2001**, *13*, 1984–1991.

(15)   Zhao, B.; Liu, D.; Peng, L.; Li, H.; Shen, P.; Xiang, N.; Liu, Y.; Tan, S. Effect of Oxadiazole Side Chains Based on Alternating Fluorene–thiophene Copolymers for Photovoltaic Cells. *Eur. Polym. J.* **2009**, *45*, 2079–2086.

(16)   Tarkuc, S.; Unver, E. K.; Udum, Y. A.; Toppare, L. Multi-Colored Electrochromic Polymer with Enhanced Optical Contrast. *Eur. Polym. J.* **2010**, *46*, 2199–2205.

(17)   Pai, C.-L.; Liu, C.-L.; Chen, W.-C.; Jenekhe, S. A. Electronic Structure and Properties of Alternating Donor–acceptor Conjugated Copolymers: 3,4-Ethylenedioxythiophene (EDOT) Copolymers and Model Compounds. *Polymer* **2006**, *47*, 699–708.

(18)   Kurach, E.; Djurado, D.; Rimarčik, J.; Kornet, A.; Wlostowski, M.; Lukeš, V.; Pécaut, J.; Zagorska, M.; Pron, A. Effect of Substituents on Redox, Spectroscopic and Structural Properties of Conjugated Diaryltetrazines - a Combined Experimental and Theoretical Study. *Phys. Chem. Chem. Phys.* **2011**, *13*, 2690–2700.

(19)   Clavier, G.; Audebert, P. S-Tetrazines as Building Blocks for New Functional Molecules and Molecular Materials. *Chem. Rev.* **2010**, *110*, 3299–3314.

(20)   Audebert, P.; Sadki, S.; Miomandre, F.; Clavier, G.; Claude Vernières, M.; Saoud, M.; Hapiot, P. Synthesis of New Substituted Tetrazines: Electrochemical and Spectroscopic Properties. *New J. Chem.* **2004**, *28*, 387-392.

(21)   Audebert, P. First Example of an Electroactive Polymer Issued from an Oligothiophene Substituted Tetrazine. *Electrochem. Commun.* **2004**, *6*, 144–147.

(22)   McCairn, M. C.; Kreouzis, T.; Turner, M. L. Microwave Accelerated Synthesis and Evaluation of Conjugated Oligomers Based on 2,5-Di-Thiophene-[1,3,4]thiadiazole. *J. Mater. Chem.* **2010**, *20*, 1999-2006.

(23)   Kurach, E.; Kotwica, K.; Zapala, J.; Knor, M.; Nowakowski, R.; Djurado, D.; Toman, P.; Pfleger, J.; Zagorska, M.; Pron, A. Semiconducting Alkyl Derivatives of 2,5-Bis(2,2'-Bithiophene-5-yl)-1,3,4-thiadiazole — Effect of the Substituent Position on the Spectroscopic, Electrochemical, and Structural Properties. *J. Phys. Chem. C* **2013**, *117*, 15316–15326.

(24)   Fisyuk, A. S.; Demadrille, R.; Querner, C.; Zagorska, M.; Bleuse, J.; Pron, A. Mixed Alkylthiophene-Based Heterocyclic Polymers Containing Oxadiazole Units via Electrochemical Polymerisation: Spectroscopic, Electrochemical and Spectroelectrochemical Properties. *New J. Chem.* **2005**, *29*, 707-713.

(25)   Grykien, R.; Luszczynska, B.; Glowacki, I.; Ulanski, J.; Kajzar, F.; Zgarian, R.; Rau, I. A Significant Improvement of Luminance vs Current Density Efficiency of a BioLED. *Opt. Mater.* **2014**, *36*, 1027–1033.

(26)   Kotwica, K.; Kurach, E.; Louarn, G.; Kostyuchenko, A. S.; Fisyuk, A. S.; Zagorska, M.; Pron, A. Alternating Copolymers of Thiadiazole and Quaterthiophenes – Synthesis,

Electrochemical and Spectroelectrochemical Characterization. *Electrochim. Acta* **2013**, *111*, 491–498.

(27) Kostyuchenko, A. S.; L.Yurpalov, V.; Kurowska, A.; Domagala, W.; Pron, A.; Fisyuk, A. S. Synthesis of New, Highly Luminescent bis(2,2'-Bithiophen-5-yl) Substituted 1,3,4-Oxadiazole, 1,3,4-Thiadiazole and 1,2,4-Triazole. *Beilstein J. Org. Chem.* **2014**, *10*, 1596–1602.

(28) Williams, A. T. R.; Winfield, S. A.; Miller, J. N. Relative Fluorescence Quantum Yields Using a Computer-Controlled Luminescence Spectrometer. *Analyst* **1983**, *108*, 1067-1071.

(29) Brouwer, A. M. Standards for Photoluminescence Quantum Yield Measurements in Solution (IUPAC Technical Report). *Pure Appl. Chem.* **2011**, *83*, 2213–2228.

(30) Frisch, M. J.; Trucks, G. W.; Schlegel, H. B.; Scuseria, G. E.; Robb, M. A.; Cheeseman, J. R.; Scalmani, G.; Barone, V.; Mennucci, B.; Petersson, G. A.; et al. Gaussian 09, revision D.01, Gaussian, Inc.: Wallingford, CT, 2009.

(31) Becke, A. D. A New Mixing of Hartree–Fock and Local Density-Functional Theories. *J. Chem. Phys.* **1993**, *98*, 1372-1377.

(32) Lee, C.; Yang, W.; Parr, R. G. Development of the Colle-Salvetti Correlation-Energy Formula into a Functional of the Electron Density. *Phys. Rev. B* **1988**, *37*, 785–789.

(33) Becke, A. D. Density-Functional Thermochemistry 3. The Role of Exact Exchange. *J. Chem. Phys.* **1993**, *98*, 5648–5652.

(34) Tomasi, J.; Mennucci, B.; Cammi, R. Quantum Mechanical Continuum Solvation Models. *Chem. Rev.* **2005**, *105*, 2999–3093.

(35) Bauernschmitt, R.; Ahlrichs, R. Treatment of Electronic Excitations within the Adiabatic Approximation of Time Dependent Density Functional Theory. *Chem. Phys. Lett.* **1996**, *256*, 454–464.

(36) Casida, M. E.; Jamorski, C.; Casida, K. C.; Salahub, D. R. Molecular Excitation Energies to High-Lying Bound States from Time-Dependent Density-Functional Response Theory: Characterization and Correction of the Time-Dependent Local Density Approximation Ionization Threshold. *J. Chem. Phys.* **1998**, *108*, 4439-4449.

(37) Stratmann, R. E.; Scuseria, G. E.; Frisch, M. J. An Efficient Implementation of Time-Dependent Density-Functional Theory for the Calculation of Excitation Energies of Large Molecules. *J. Chem. Phys.* **1998**, *109*, 8218-8224.

(38) Van Caillie, C.; Amos, R. D. Geometric Derivatives of Excitation Energies Using SCF and DFT. *Chem. Phys. Lett.* **1999**, *308*, 249–255.

(39) Van Caillie, C.; Amos, R. D. Geometric Derivatives of Density Functional Theory Excitation Energies Using Gradient-Corrected Functionals. *Chem. Phys. Lett.* **2000**, *317*, 159–164.

(40) Furche, F.; Ahlrichs, R. Adiabatic Time-Dependent Density Functional Methods for Excited State Properties. *J. Chem. Phys.* **2002**, *117*, 7433-7447.

(41) Scalmani, G.; Frisch, M. J.; Mennucci, B.; Tomasi, J.; Cammi, R.; Barone, V. Geometries and Properties of Excited States in the Gas Phase and in Solution: Theory and Application of a Time-Dependent Density Functional Theory Polarizable Continuum Model. *J. Chem. Phys.* **2006**, *124*, 094107-1 - 094107-15.

(42) O'Boyle, N. M.; Tenderholt, A. L.; Langner, K. M. Cclib: A Library for Package-Independent Computational Chemistry Algorithms. *J. Comput. Chem.* **2008**, *29*, 839–845.

(43) Allouche, A.-R. Gabedit--a Graphical User Interface for Computational Chemistry Softwares. *J. Comput. Chem.* **2011**, *32*, 174–182.

(44) Improta, R.; Barone, V.; Scalmani, G.; Frisch, M. J. A State-Specific Polarizable Continuum Model Time Dependent Density Functional Theory Method for Excited State Calculations in Solution. *J. Chem. Phys.* **2006**, *125*, 054103-1 - 054103-9.

(45) Improta, R.; Scalmani, G.; Frisch, M. J.; Barone, V. Toward Effective and Reliable Fluorescence Energies in Solution by a New State Specific Polarizable Continuum Model Time Dependent Density Functional Theory Approach. *J. Chem. Phys.* **2007**, *127*, 074504-1 - 074504-9.

(46) Kudin, K. N.; Scuseria, G. E. A Fast Multipole Algorithm for the Efficient Treatment of the Coulomb Problem in Electronic Structure Calculations of Periodic Systems with Gaussian Orbitals. *Chem. Phys. Lett.* **1998**, *289*, 611–616.

(47) Kudin, K.; Scuseria, G. Linear-Scaling Density-Functional Theory with Gaussian Orbitals and Periodic Boundary Conditions: Efficient Evaluation of Energy and Forces via the Fast Multipole Method. *Phys. Rev. B* **2000**, *61*, 16440–16453.

(48) Mitschke, U.; Debaerdemaeker, T.; Bäuerle, P. Structure-Property Relationships in Mixed Oligoheterocycles Based on End-Capped Oligothiophenes. *European J. Org. Chem.* **2000**, *2000*, 425–437.

(49) Ramsden, C. A. The Influence of Aza-Substitution on Azole Aromaticity. *Tetrahedron* **2010**, *66*, 2695–2699.

(50) Zak, J.; Lapkowski, M.; Guillerez, S.; Bidan, G. Electrochemistry and Spectroelectrochemistry of Regioregular Oligooctylthiophenes. *Synth. Met.* **2005**, *152*, 185–188.

(51) Ponce Ortiz, R.; Casado, J.; Hernández, V.; López Navarrete, J. T.; Letizia, J. A.; Ratner, M. A.; Facchetti, A.; Marks, T. J. Thiophene-Diazine Molecular Semiconductors: Synthesis, Structural, Electrochemical, Optical, and Electronic Structural Properties; Implementation in Organic Field-Effect Transistors. *Chemistry* **2009**, *15*, 5023–5039.

(52) Qu, S.; Chen, X.; Shao, X.; Li, F.; Zhang, H.; Wang, H.; Zhang, P.; Yu, Z.; Wu, K.; Wang, Y.; et al. Self-Assembly of Highly Luminescent Bi-1,3,4-Oxadiazole Derivatives through

Electron Donor–acceptor Interactions in Three-Dimensional Crystals, Two-Dimensional Layers and Mesophases. *J. Mater. Chem.* **2008**, *18*, 3954-3964.

(53)   Caarls, W.; Soledad Celej, M.; Demchenko, A. P.; Jovin, T. M. Characterization of Coupled Ground State and Excited State Equilibria by Fluorescence Spectral Deconvolution. *J. Fluoresc.* **2010**, *20*, 181–190.

(54)   Rybakiewicz, R.; Gawrys, P.; Tsikritzis, D.; Emmanouil, K.; Kennou, S.; Zagorska, M.; Pron, A. Electronic Properties of Semiconducting Naphthalene Bisimide derivatives—Ultraviolet Photoelectron Spectroscopy versus Electrochemistry. *Electrochim. Acta* **2013**, *96*, 13–17.

(55)   Erdem, S. S.; Özpınar, G. A.; Saçan, M. T. Investigation on the Aromaticity of 1,3,4-Thiadiazole-2-Thione and Its Oxygen Analogs Including Their Tautomeric Forms. *J. Mol. Struct. THEOCHEM* **2005**, *726*, 233–243.

(56)   Sek, D.; Bijak, K.; Grucela-Zajac, M.; Filapek, M.; Skorka, L.; Siwy, M.; Janeczek, H.; Schab-Balcerzak, E. Synthesis and Study on the Light Absorbing, Emitting, Redox and Electrochromic Properties of Azines and Polyazines with Thiophene Units. *Synth. Met.* **2012**, *162*, 1623–1635.

(57)   Krompiec, S.; Filapek, M.; Grudzka, I.; Kula, S.; Słodek, A.; Skórka, Ł.; Danikiewicz, W.; Ledwon, P.; Lapkowski, M. An Ambipolar Behavior of Novel Ethynyl-Bridged polythiophenes—A Comprehensive Study. *Synth. Met.* **2013**, *165*, 7–16.

(58)   Zade, S. S.; Bendikov, M. From Oligomers to Polymer: Convergence in the HOMO-LUMO Gaps of Conjugated Oligomers. *Org. Lett.* **2006**, *8*, 5243–5246.

(59)   Zade, S. S.; Zamoshchik, N.; Bendikov, M. From Short Conjugated Oligomers to Conjugated Polymers. Lessons from Studies on Long Conjugated Oligomers. *Acc. Chem. Res.* **2011**, *44*, 14–24.

(60)   Audebert, P.; Catel, J.-M.; Le Coustumer, G.; Duchenet, V.; Hapiot, P. Electrochemistry and Polymerization Mechanisms of Thiophene−Pyrrole−Thiophene Oligomers and Terthiophenes. Experimental and Theoretical Modeling Studies. *J. Phys. Chem. B* **1998**, *102*, 8661–8669.

(61)   Guay, J.; Kasai, P.; Diaz, A.; Wu, R.; Tour, J. M.; Dao, L. H. Chain-Length Dependence of Electrochemical and Electronic Properties of Neutral and Oxidized Soluble α,α-Coupled Thiophene Oligomers. *Chem. Mater.* **1992**, *4*, 1097–1105.

(62)   Demanze, F.; Yassar, A.; Garnier, F. Alternating Donor−Acceptor Substitutions in Conjugated Polythiophenes. *Macromolecules* **1996**, *29*, 4267–4273.

(63)   Fraind, A. M.; Sini, G.; Risko, C.; Ryzhkov, L. R.; Brédas, J.-L.; Tovar, J. D. Charge Delocalization through Benzene, Naphthalene, and Anthracene Bridges in Π-Conjugated Oligomers: An Experimental and Quantum Chemical Study. *J. Phys. Chem. B* **2013**, *117*, 6304–6317.

(64) Yamamoto, T.; Kanbara, T.; Mori, C.; Wakayama, H.; Fukuda, T.; Inoue, T.; Sasaki, S. Vacuum-Deposited Thin Film of Linear Π - Conjugated Poly(arylene)s. Optical, Electrochemical, and Electrical Properties and Molecular Alignment. *J. Phys. Chem.* **1996**, *100*, 12631–12637.

(65) Kobayashi, M.; Chen, J.; Chung, T.-C.; Moraes, F.; Heeger, A. J.; Wudl, F. Synthesis and Properties of Chemically Coupled Poly(thiophene). *Synth. Met.* **1984**, *9*, 77–86.

(66) McCullough, R. D. The Chemistry of Conducting Polythiophenes. *Adv. Mater.* **1998**, *10*, 93–116.

(67) Mastragostino, M.; Soddu, L. Electrochemical Characterization of "n" Doped Polyheterocyclic Conducting polymers—I. Polybithiophene. *Electrochim. Acta* **1990**, *35*, 463–466.

(68) Yamamoto, T.; Suganuma, H.; Maruyama, T.; Inoue, T.; Muramatsu, Y.; Arai, M.; Komarudin, D.; Ooba, N.; Tomaru, S.; Sasaki, S.; et al. Π-Conjugated and Light Emitting Poly(4,4'-Dialkyl-2,2'-Bithiazole-5,5'-Diyl)s and Their Analogues Comprised of Electron-Accepting Five-Membered Rings. Preparation, Regioregular Structure, Face-to-Face Stacking, and Electrochemical and Optical Properties. *Chem. Mater.* **1997**, *9*, 1217–1225.

(69) Bredas, J. L.; Street, G. B. Polarons, Bipolarons, and Solitons in Conducting Polymers. *Acc. Chem. Res.* **1985**, *18*, 309–315.

(70) Zade, S. S.; Bendikov, M. Theoretical Study of Long Oligothiophene Polycations as a Model for Doped Polythiophene. *J. Phys. Chem. C* **2007**, *111*, 10662–10672.

(71) Zamoshchik, N.; Salzner, U.; Bendikov, M. Nature of Charge Carriers in Long Doped Oligothiophenes: The Effect of Counterions. *J. Phys. Chem. C* **2008**, *112*, 8408–8418.

(72) Zade, S. S.; Bendikov, M. Theoretical Study of Long Oligothiophene Dications: Bipolaron vs Polaron Pair vs Triplet State. *J. Phys. Chem. B* **2006**, *110*, 15839–15846.

(73) Pokrop, R.; Verilhac, J.-M.; Gasior, A.; Wielgus, I.; Zagorska, M.; Travers, J.-P.; Pron, A. Effect of Molecular Weight on Electronic, Electrochemical and Spectroelectrochemical Properties of poly(3,3'-Dioctyl-2,2':5',2'-Terthiophene). *J. Mater. Chem.* **2006**, *16*, 3099-3106.

(74) Salzner, U. Investigation of Charge Carriers in Doped Thiophene Oligomers through Theoretical Modeling of Their UV/Vis Spectra. *J. Phys. Chem. A* **2008**, *112*, 5458–5466.

(75) Alkan, F.; Salzner, U. Theoretical Investigation of Excited States of Oligothiophene Anions. *J. Phys. Chem. A* **2008**, *112*, 6053–6058.

(76) Okur, S.; Salzner, U. Theoretical Modeling of the Doping Process in Polypyrrole by Calculating UV/Vis Absorption Spectra of Neutral and Charged Oligomers. *J. Phys. Chem. A* **2008**, *112*, 11842–11853.

(77) Zykwinska, A.; Domagala, W.; Czardybon, A.; Pilawa, B.; Lapkowski, M. In Situ EPR Spectroelectrochemical Studies of Paramagnetic Centres in poly(3,4-

Ethylenedioxythiophene) (PEDOT) and poly(3,4-Butylenedioxythiophene) (PBuDOT) Films. *Chem. Phys.* **2003**, *292*, 31–45.

(78) Zykwinska, A.; Domagala, W.; Lapkowski, M. ESR Spectroelectrochemistry of poly(3,4-Ethylenedioxythiophene) (PEDOT). *Electrochem. Commun.* **2003**, *5*, 603–608.

(79) Lukeš, V.; Rapta, P.; Idzik, K. R.; Beckert, R.; Dunsch, L. Charged States of 1,3,5-Triazine Molecules as Models for Star-Shaped Molecular Architecture: A DFT and Spectroelectrochemical Study. *J. Phys. Chem. B* **2011**, *115*, 3344–3353.

(80) Cravino, A.; Neugebauer, H.; Luzzati, S.; Catellani, M.; Petr, A.; Dunsch, L.; Sariciftci, N. S. Positive and Negative Charge Carriers in Doped or Photoexcited Polydithienothiophenes: A Comparative Study Using Raman, Infrared, and Electron Spin Resonance Spectroscopy. *J. Phys. Chem. B* **2002**, *106*, 3583–3591.

(81) Baibarac, M.; Lapkowski, M.; Pron, A.; Lefrant, S.; Baltog, I. SERS Spectra of poly(3-Hexylthiophene) in Oxidized and Unoxidized States. *J. Raman Spectrosc.* **1998**, *29*, 825–832.

(82) Agosti, E.; Rivola, M.; Hernandez, V.; Del Zoppo, M.; Zerbi, G. Electronic and Dynamical Effects from the Unusual Features of the Raman Spectra of Oligo and Polythiophenes. *Synth. Met.* **1999**, *100*, 101–112.

(83) Louarn, G.; Buisson, J. P.; Lefrant, S.; Fichou, D. Vibrational Studies of a Series of α-Oligothiophenes as Model Systems of Polythiophene. *J. Phys. Chem.* **1995**, *99*, 11399–11404.

Table of contents image: